Regional Differences of Choroidal Structure Determined by Wide-Field Optical Coherence Tomography

Naoko Kakiuchi, Hiroto Terasaki, Shozo Sonoda, Hideki Shiihara, Takehiro Yamashita, Masatoshi Tomita, Yuki Shinohara, Tomonori Sakoguchi, Kazuhiro Iwata, and Taiji Sakamoto

Department of Ophthalmology, Kagoshima University Graduate School of Medical and Dental Sciences, Kagoshima, Japan

Correspondence: Taiji Sakamoto, Department of Ophthalmology, Kagoshima University Graduate School of Medical and Dental Sciences, 8-35-1 Sakuragaoka, Kagoshima-shi, Kagoshima, 890-0075, Japan; tsakamot@m3.kufm.kagoshima-u.ac.jp.

Submitted: March 8, 2018
Accepted: May 13, 2019

Citation: Kakiuchi N, Terasaki H, Sonoda S, et al. Regional differences of choroidal structure determined by wide-field optical coherence tomography. *Invest Ophthalmol Vis Sci*. 2019;60:2614–2622. https://doi.org/10.1167/iovs.18-24296

Purpose. To compare the submacular to the perimacular choroidal structure in images obtained by wide-field optical coherence tomography (OCT).

Methods. Thirty eyes of 30 healthy volunteers (15 men) were studied. Twelve wide-field radial circumferential scans were recorded with enhanced depth imaging OCT from the macular and perimacular zones. The sizes of the luminal and stromal areas of the choroid were determined. The two zones were subdivided into the superior, inferior, nasal, and temporal sectors. The total choroidal area, the luminal and stromal areas, and the luminal ratio of each sector were compared.

Results. All of the choroidal structural parameters analyzed in the present study were largest in the superior sector followed by the temporal, inferior, and nasal sectors. The coefficients of variation were larger in the perimacular zone than in the macular zone: The luminal ratio in the macular zone varied by 1.2%, and that in perimacular zone varied by 4.2%.

Conclusions. The variations in the ratios of the luminal areas of the choroid in the wide-field OCT images are slight in the macular zone but considerable in the perimacular zone.

Keywords: choroid structure, widefield OCT, EDI-OCT

The choroid plays an important role in maintaining the homeostasis of the retinochoroidal tissues.[1–3] There is increasing evidence that the choroid is altered in different types of retinochoroidal diseases,[4–12] and also in different hydration and oxidation states.[13] Methods are being developed to quantify these alterations.

In the optical coherence tomography (OCT) image, the choroid has two main structural components: the stromal areas and the vascular or luminal areas. However, it is difficult to quantify the stromal and luminal areas separately because they are not architecturally separated.

A wide-field ocular fundus imaging system was recently introduced, and this system has enabled clinicians to examine a large area of the ocular fundus in one image.[14,15] Investigations with this wide-field fundus imaging system have provided important information on the changes in the more peripheral retina and choroid in many types of retinochoroidal diseases.[16–18] For example, pathological changes have been detected in the peripheral retina of eyes with central serous chorioretinopathy (CSC) and Vogt-Koyanagi-Harada disease more frequently than was believed.[16,18,19] Because it is highly likely that analysis of wide-field fundus images will become more informative in evaluating retinal diseases, normative values of the wide-field OCT images need to be obtained. However, the choroidal structure in wider areas around macula is not well studied.[20]

In 2013, we developed a method to measure the areas of the lumen and stroma of the choroid separately in OCT images.[10,11] Subsequently, many researchers have used this technique and have reported that specific structural changes can be associated with the progression of various ocular diseases.[10–12,21–31]

Recently, there have been several reports on the choroidal structure in OCT images. Branchini et al.[32] reported that the choroidal luminal area was larger than the stromal area. Agrawal et al.[33] reported that 66% of the choroid was composed of luminal apace using a binarization method to determine the choroidal vascularity index (CVI). Kajić et al.[34] constructed three-dimensional images of the choroidal structures, and Esmaeelpour et al.[35] reported on an autosegmentation technique to divide Sattler's and Haller's layer.

However, the examined area in these studies was limited to the choroid beneath the central macula (i.e., the submacular choroid). As best we know, the normative values of the stromal and luminal choroid in the perimacular region of normal eyes have not been determined.

Thus, the purpose of this study was to analyze the structure of the choroid in a more peripheral area in normal eyes of healthy subjects. To accomplish this, we obtained wide-field images of the retina and choroid of 30 healthy eyes and analyzed the images with the binarization method. We shall show that there are significant regional differences in the normal human choroid. This information will be indispensable not only for understanding the properties of healthy choroids but also in interpreting the changes in the choroid of diseased eyes.

Methods

This was a cross-sectional, prospective study of 30 eyes of 30 healthy volunteers. The procedures used in this study were approved by the Ethics Committee of Kagoshima University Hospital (Kagoshima, Japan). A written informed consent was

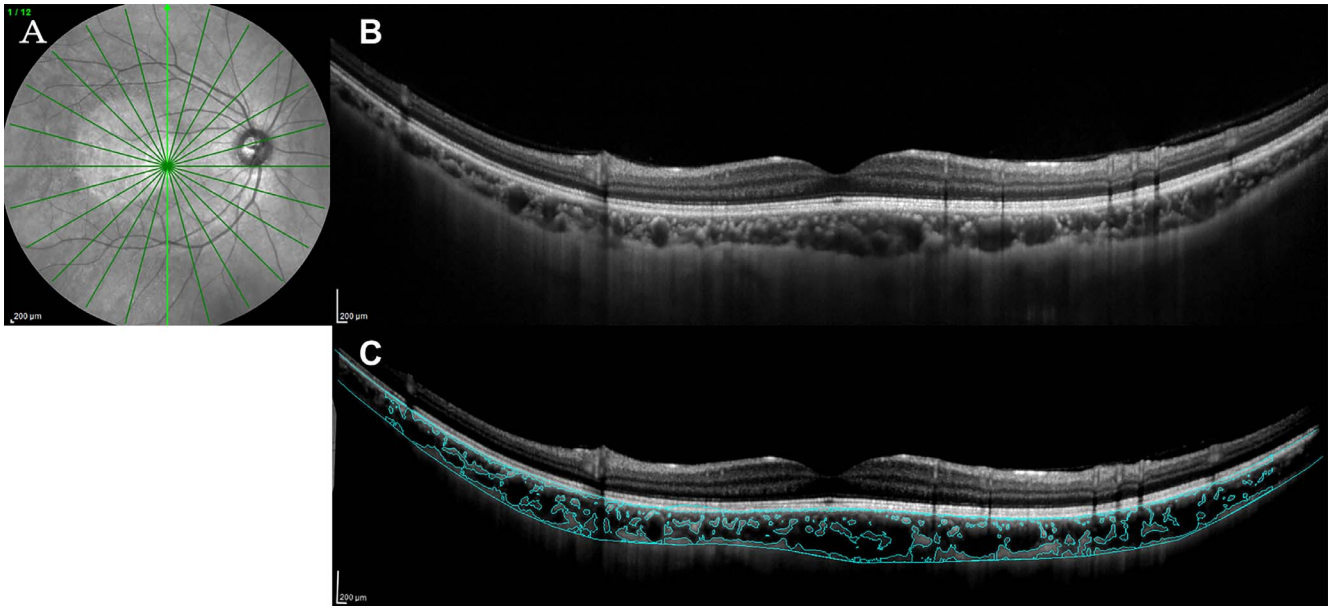

FIGURE 1. Images illustrating the binarization method applied on the choroidal portion of OCT scans. (**A**) Infrared reflectance image with the orientation of the 12 scans projected on it. (**B**) Representative radial wide-field OCT image (vertical scan). (**C**) Overlay of binarization by ImageJ separating stromal (*cyan*) and luminal areas.

obtained from all the subjects after an explanation of the procedures to be used and the possible complications. All of the procedures conformed to the tenets of the Declaration of Helsinki.

Prior to the measurements, all of the eyes had a comprehensive ocular examination, which included slit-lamp examinations of the anterior segment of the eye and ophthalmoscopic examinations of the fundus. The intraocular pressure was measured with a pneumotonometer (CT-80; Topcon, Tokyo, Japan), and the axial length was measured with the AL-2000 ultrasound instrument (Tomey, Tokyo, Japan). The best-corrected visual acuity (BCVA) was measured after determining the refractive error (spherical equivalent) with an Auto Kerato-Refractometer (RM8900, Topcon). If both eyes met the inclusion criteria, only the right eye was analyzed.

The eligibility criteria were; age $\geq$20 years, and eyes confirmed to be normal by ophthalmic examinations including ophthalmoscopy and OCT. The exclusion criteria were eyes with known ocular diseases such as glaucoma and diabetic retinopathy, presence of systemic diseases such as hypertension and diabetes, high myopia of more than –6.0 diopters (D), prior intraocular surgery or injections, or eyes in which the ocular fundus could not be observed due to media opacities. None of the eyes were excluded due to poor-quality OCT images because of poor fixation.

Choroidal Images Measured by Spectral-Domain Optical Coherence Tomography (SD-OCT)

Wide-field enhanced depth imaging (EDI)-OCT images were obtained with the Spectralis HRA + OCT instrument (Heidelberg Engineering, Heidelberg, Germany) with a 55° lens as described in detail in our earlier publications.[10,11] These images were taken by experienced examiners and the refractive error of each subject was entered into the embedded adjustor to minimize the error of the scale of each image. The validity of this method in lateral scaling was confirmed in the HRT instrument.[36] The scans were 12 circumferential radial lines through the center of the fovea (Fig. 1). The images of 24 scanning planes with 15° angles between each plane were recorded. Each image was obtained using the eye tracking system, and 100 scans were averaged. All of the eyes were examined without mydriasis with a 1-hour interval between measurements, and all recordings were made between 3 PM and 5 PM to avoid the effects of diurnal fluctuations of the choroidal thickness.

Analysis of OCT Images

The luminal and the stromal areas of the choroid were measured by a binarization method (Fig. 1).[31,37] Briefly, the OCT images were analyzed with the ImageJ software (version 1.47; National Institutes of Health, Bethesda, MD, USA).[38] A region of interest (ROI) was selected and set by the ROI manager in the OCT image. Then, three choroidal vessels with lumens larger than 100 µm were randomly selected by the oval selection tool of the tool bar, and the average reflectivity of these areas was determined by the software. The average brightness of three luminal areas was set as the minimum value to minimize the noise. Then, the image was converted to 8-bit images and adjusted by the auto local threshold of Niblack. The binarized image was reconverted to the conventional RGB images for display purposes, and the luminal area was determined with the threshold tool. After adding the information on the distance between two pixels, the total choroidal area, luminal area, and stromal area were automatically calculated. The light pixels were defined as the stromal choroid or choroidal interstitial area and the dark pixels were defined as the luminal area. The stromal choroid consists of the vessel walls and other tissues such as connective tissues, myocytes, nerve fibers, and inflammatory cells, among others.[39]

Comparison of Choroidal Structure in Macular and Perimacular Zones

To study the choroidal structure in different areas, we divided the choroidal areas by their locations. First, we classified the area within the 3000 µm from the fovea as the macular zone, and the area peripheral to the macular zone as the perimacular zone, which was 3000 µm from the fovea and had a radius of

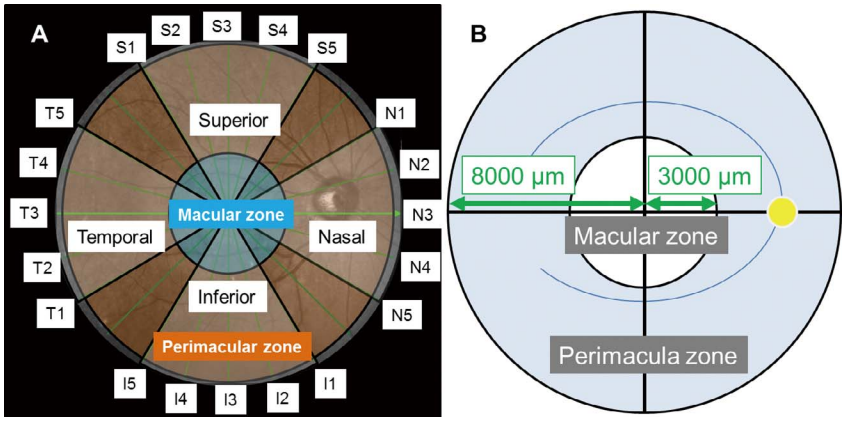

Figure 2. Schematic drawing showing macular and perimacular zones and each sector in the wide-field EDI-OCT images. (**A**) The OCT image was divided into the macular zone, which was within 3000 μm from the fovea, and the perimacular zone, which was located 3000- to 8000-μm radius from the fovea. (**B**) Each zone was further divided into a superior, inferior, nasal, and temporal sector.

8000 μm (Fig. 2). Next, we divided each zone into superior, inferior, nasal, and temporal sectors (Fig. 2). The value of each structural parameter of one sector was calculated as the average of the five different scans of each sector (e.g., scanning planes S1–S5 for the superior sector).

Then, we compared the total area, stromal area, and luminal area of each sector of the choroid in the macular and perimacular zones. Because the scanned width was different between the macular (3000 μm) and the perimacular zone (5000 μm), each parameter was expressed as the area $mm^2/10^3$ μm.

Comparison of Choroidal Structure in Superior and Inferior Sectors in Macular and Perimacular Zones

The choroid in superior and inferior sectors is vascularized differently, which is determined by a horizontal watershed zone around the fovea.[40] Thus, we compared the choroidal structure in the superior and inferior sectors in the macular and the perimacular zones. The following formula was used to quantify the value of the degree of vascularization.

Difference of Cross-Sectional Area = (Total Choroidal Area per 10^3-μm Width of Scanned OCT Image in Superior Area) − (Total Choroidal Area per 10^3-μm Width of Scanned OCT Image in Corresponding Inferior Area) (Fig. 3).

Coefficients of Variation of Macular and Perimacular Zones

The coefficient of variation (CV) of each parameter was calculated by dividing the standard deviation by the average (SD/average) in the macular and perimacular zones.

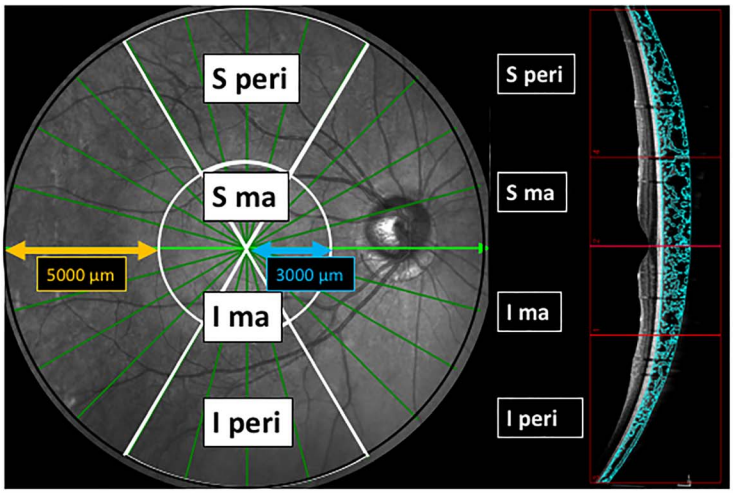

$$\text{Difference of size per cross sectional area in macular zone (per } 10^3\ \mu m) = \frac{\text{Area of A } (mm^2) - \text{Area of B } (mm^2)}{3}$$

$$\text{Difference of size per cross sectional area in perimacular zone (per } 10^3\ \mu m) = \frac{\text{Area of C } (mm^2) - \text{Area of D } (mm^2)}{5}$$

Figure 3. Schematic image for comparisons of the choroidal structure between the superior and inferior sectors. Scanning laser ophthalmoscopic (SLO) and optical coherence tomographic (OCT) images of a vertical scan are shown. (*Right*) SLO images corresponding to the OCT images. The choroidal areas of the superior and inferior sectors in the macular and perimacular zones are compared by a formula (see Methods). S peri, superior in the perimacular zone; S ma, superior in the macular zone; I ma, inferior in the macular zone; I peri, inferior in the perimacular zone.

Table 1. Background of Participants

Characteristics	Mean ± SD	Range
Age, y	34.4 ± 8.48	22 to 57
Male/female, *n*	15/15	
Spherical equivalent, D	−2.68 ± 1.68	−5.875 to −0.25
Axial length, mm	24.81 ± 1.15	21.09 to 26.67

Statistical Analyses

Statistical analyses were performed with the SPSS 23 for Windows software (SPSS, Inc., IBM, Somers, NY, USA) or the EZR software (Saitama Medical Center, Jichi Medical University, Saitama, Japan).[41] Friedman tests were used to compare the choroidal area and structure among the four sectors. The following multiple test was done using the Bonferroni method. The correlations between the different cross-sectional choroidal parameters, namely, the total area, luminal area, stromal area, luminal/stromal ratio, and the age, sex, axial length, and refractive error were determined by Spearman correlation analyses. The Mann-Whitney *U* test was used to determine the CV in the macular zone and in the perimacular zone. The Wilcoxon signed ranks test was used to determine the significance of the differences of the superior and inferior sectors of the different choroidal parameters. A P value < 0.05 was considered to be statistically significant.

Results

Demographics of Volunteers

The average age of the volunteers was 34.4 ± 8.48 years (average ± SD) with a range of 22 to 57 years (Table 1). The mean axial length was 24.81 ± 1.15 mm with a range of 21.09 to 26.67 mm. The mean refractive error (spherical equivalent) was –2.68 ± 1.68 D with a range of –5.87 to –0.25 D.

Choroidal Structure in Macular Zone

The total choroidal, luminal, and stromal areas in each sector of the macular zone are shown in Figure 4 and Table 2. The largest area was the superior sector followed by the temporal, inferior, and nasal sectors. The largest luminal area was the superior sector followed by the temporal, inferior, and nasal sectors. The average of the total choroidal area was significantly different among the sectors, ranging from 0.28 to 0.34 $mm^2/10^3$ µm for the total choroidal area, from 0.19 to 0.24 $mm^2/10^3$ µm for the luminal area, and from 0.09 to 0.11 $mm^2/10^3$ µm for the stromal areas. The ratio of the luminal/stromal areas for each sector ranged from 66.75% to 67.91%, and none was significantly different from the others (Table 2). Although the luminal area differed significantly in the different sectors, the luminal ratio was not significantly different.

Choroidal Structure in Perimacular Zone

The largest total choroidal area was 0.30 $mm^2/10^3$ µm in the superior sector followed by the temporal, inferior, and nasal sectors (Fig. 4; Table 3). In the luminal and stromal areas, the largest area was the superior sector followed by the temporal, inferior, and nasal sectors. The average total choroidal area was significantly different between sectors, ranging from 0.20 to 0.30 $mm^2/10^3$ µm for the total choroidal area, from 0.12 to 0.20 $mm^2/10^3$ µm for the luminal area, and from 0.07 to 0.10 $mm^2/10^3$ µm for the stromal area. The luminal ratio (luminal area/total choroidal area) of the sectors ranged from 61.94% to 66.08% with significant differences. The mean luminal area was 0.08 $mm^2/10^3$ µm, which was significantly larger than that of the stromal area at 0.03 $mm^2/10^3$ µm.

Comparisons of Choroidal Structures of Superior and Inferior Sectors

The difference of the total choroidal area between the superior and inferior sectors was 0.03 ± 0.04 $mm^2/10^3$ µm in the macular zone and 0.07 ± 0.04 $mm^2/10^3$ µm in the perimacular zone. The difference was significantly larger in the perimacular zone than in the macular zone ($P > 0.001$, Table 4). The difference between the superior and inferior sectors in the perimacular zone was significantly larger than that in macular zone for the luminal and stromal areas (0.02 vs. 0.005 $mm^2/10^3$ µm for the luminal area [$P = 0.009$]; 0.005 vs. 0.02 $mm^2/10^3$ µm for the stromal area [$P < 0.001$]).

Table 2. Regional Difference of Choroidal Parameters in Macular Area

Macular Zone	Total Choroidal Areas, $mm^2/10^3$ µm	Luminal Area, $mm^2/10^3$ µm	Stromal Area, $mm^2/10^3$ µm	Luminal Ratio, %
Superior	0.34 ± 0.07	0.24 ± 0.06	0.11 ± 0.02	67.91 ± 2.57
Inferior	0.32 ± 0.07	0.21 ± 0.05	0.10 ± 0.02	66.75 ± 2.66
Nasal	0.28 ± 0.07	0.19 ± 0.06	0.09 ± 0.02	67.83 ± 2.43
Temporal	0.32 ± 0.07	0.21 ± 0.05	0.10 ± 0.02	67.23 ± 2.00

P values using Bonferroni test.
* $P < 0.05$.
† $P < 0.01$.
N.S.

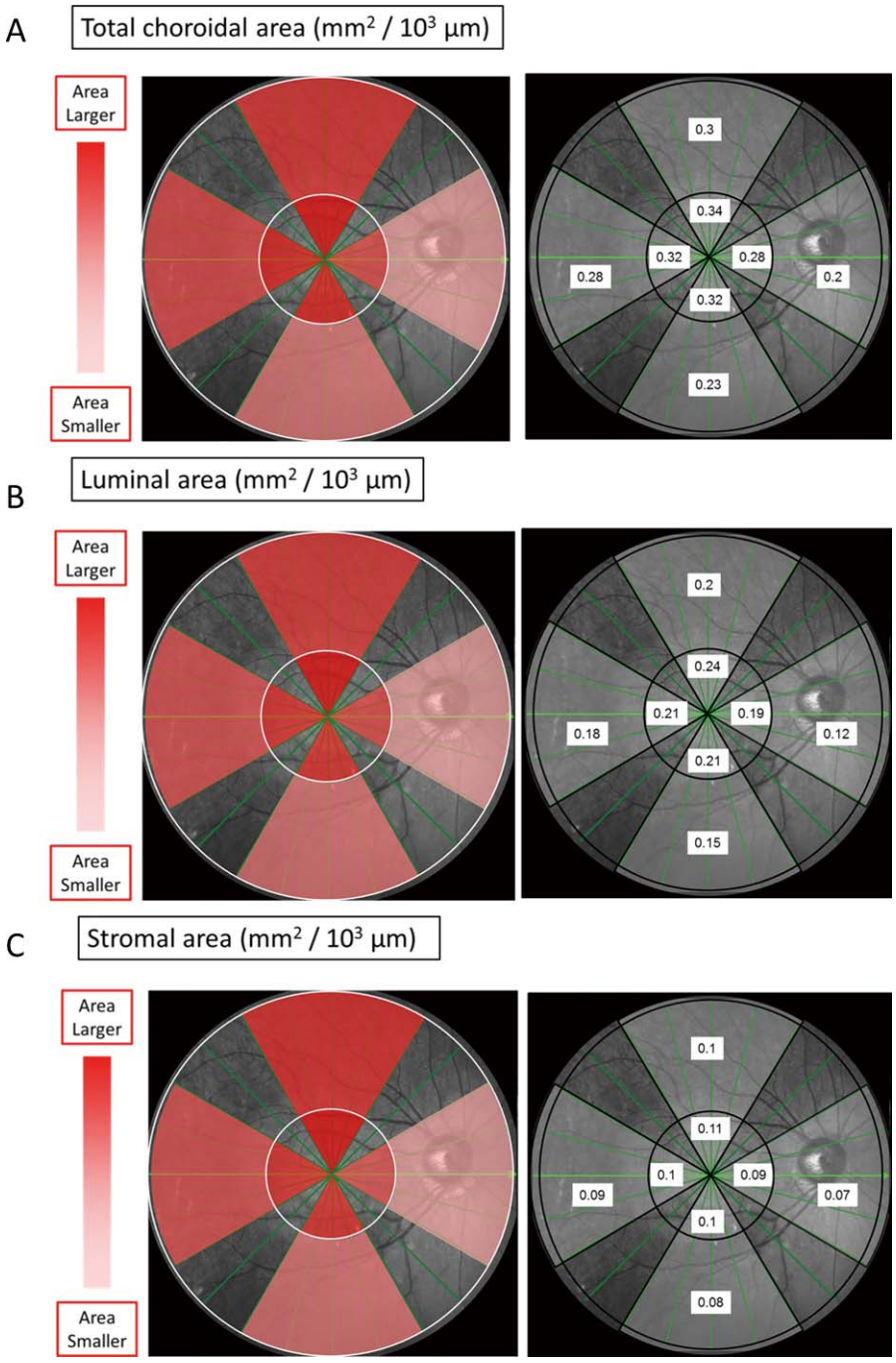

Figure 4. Color map of total choroidal area (**A**), luminal area (**B**), and stromal area (**C**). The size of each area is shown by the color saturation at *left*. Absolute numerical value of area per 10^3 µm of each sector is shown at *left* ($mm^2/10^3$ µm).

Differences of Total Choroidal Area and Stroma/Luminal Ratio in Macular and Perimacular Zones

In the macular zone, the total choroidal area ranged from 0.28 $mm^2/10^3$ µm in the nasal sector to 0.35 $mm^2/10^3$ µm in the superior sector. Thus, the superior sector was 25% larger than the nasal sector (Fig. 5; absolute value is shown in Supplementary Table S1). This difference was also found for the luminal and stromal areas with a range of 0.19 to 0.24 $mm^2/10^3$ µm, a 26.3% difference for the luminal area, and 0.09 to 0.11 $mm^2/10^3$ µm, a 22.2% difference, for the stromal area. Thus, the luminal ratio was not significantly different in any sector in the macular zone and ranged from 66.67% in the inferior sector to 68.97% in the superior sector for a difference of 2.3% (Fig. 5; Supplementary Fig. S1).

The variations of the choroidal structure in the perimacular zone was larger than that in the macular zone (Fig. 5). Thus, the total choroidal area varied from 0.18 $mm^2/10^3$ µm in the nasal sector to 0.34 $mm^2/10^3$ in the superior sector, a difference of 88%. The stromal area varied from 0.07 to 0.10 $mm^2/10^3$ µm, a difference of 42.9%. The variations in the luminal area ranged from 0.11 to 0.24 $mm^2/10^3$ µm, a difference of 118%, which was significantly larger than that of the stromal area. The luminal ratio ranged from 61.11% in

Table 3. Regional Difference of Choroidal Parameters in Perimacular Area

Macular Zone	Total Choroidal Areas, $mm^2/10^3$ µm	Luminal Area, $mm^2/10^3$ µm	Stromal Area, $mm^2/10^3$ µm	Luminal Ratio, %
Superior	0.30 ± 0.06 †, †, *, †	0.20 ± 0.04 †, †, *, †	0.10 ± 0.02 †, †, *, †	66.08 ± 2.21 †, †, †
Inferior	0.23 ± 0.04 †, †, *, †	0.15 ± 0.03 †, †, *, †	0.08 ± 0.01 †, †, *, †	63.42 ± 2.60 †, †, †
Nasal	0.20 ± 0.04 †, †, *, †	0.12 ± 0.03 †, †, *, †	0.07 ± 0.01 †, †, *, †	61.94 ± 2.83 †, †, †
Temporal	0.28 ± 0.05	0.18 ± 0.04	0.09 ± 0.01	65.67 ± 2.50

P values using Bonferroni test.
* $P < 0.05$.
† $P < 0.01$.

the nasal sector to 70.59% in the superior sector, a 9.48% difference.

Coefficients of Variation

The CV of the total choroidal area in the perimacular zone was 0.22, which was significantly larger than that in macular zone of 0.07 ($P < 0.001$; Table 5). The CV of the luminal area in the perimacular zone was 0.12, which was significantly larger than the 0.07 of the macular zone (0.07, $P < 0.001$; Table 5). The CV of the stromal area in the perimacular zone was also significantly larger than in the macular zone (0.04 vs. 0.08, $P = 0.002$; Table 5). Thus, the CV of the luminal ratio in the perimacular zone was significantly larger than that in the macular zone.

Relationship Between Age, Axial Length, Refractive Error, and Parameters of Macular and Perimacular Zones

Age, axial length, sex, and refractive error have been reported to be significantly correlated with the choroidal thickness.[41,42] Thus, we performed multiple regression analysis between each one of these factors and the choroidal parameters. Several parameters, especially in the perimacular zone, were significantly correlated with age (Supplementary Table S3). Axial length, sex, and refractive error were not significantly correlated with any of the choroidal parameters in the macular and perimacular zones (data not shown).

Discussion

We have analyzed the structure of the choroid in the macular zone and the perimacular zone using the binarized image processing technique on high-penetration OCT images.[10,11,21–29,31] The results showed that the total choroidal area and the luminal ratios were significantly larger in the macular zone than in the perimacular zone. This confirms the results of an earlier study that reported that the macular choroid was thicker than the peripheral choroid.[42,43] However, our findings also showed that the thickness was due to an increase in the size of the lumens of the blood vessels.

Each of the choroidal structural parameters had greater variations in the perimacular sectors than in the macular sectors. This means that the choroid in the macular zone has not only larger vascular lumens, but also a more uniform luminal rate than that in the perimacular zone. This difference was largely due to the differences of the luminal area rather than the stromal area. In the macular area, the photoreceptor density is highest,[44,45] and thus outer nuclear layer is thickest.[45] All this taken together, there is higher metabolic need in the macular area, and thus the macular retina requires higher blood circulation than the peripheral retina. In addition, there is the asymmetric dorsoventral gradient in photoreceptor density in the posterior pole of the retina.[44] This asymmetricity might affect the greater variations of choroidal parameters in the perimacular zone.

We further compared the areas of the different sectors in the two zones. In both the macular and perimacular zones, the superior area was always the largest and the nasal sector was

Table 4. Difference of Choroidal Parameters Between Superior and Inferior Sector

Parameter	Macular Zone, Mean ± SD	Perimacular Zone, Mean ± SD	*P* Value‡
Total choroid area, $mm^2/10^3$ µm	0.03 ± 0.04*	0.07 ± 0.04†	<0.01
Luminal area, $mm^2/10^3$ µm	0.02 ± 0.04*	0.05 ± 0.03†	<0.01
Stromal area, $mm^2/10^3$ µm	0.005 ± 0.0*	0.02 ± 0.01†	<0.01
Luminal ratio, %	1.16 ± 2.78	2.66 ± 2.56†	<0.01

P values for comparison of choroidal structure between superior and inferior sector using Bonferroni test.
* $P < 0.05$.
† $P < 0.01$.
‡ *P* values using Wilcoxon signed ranks test.

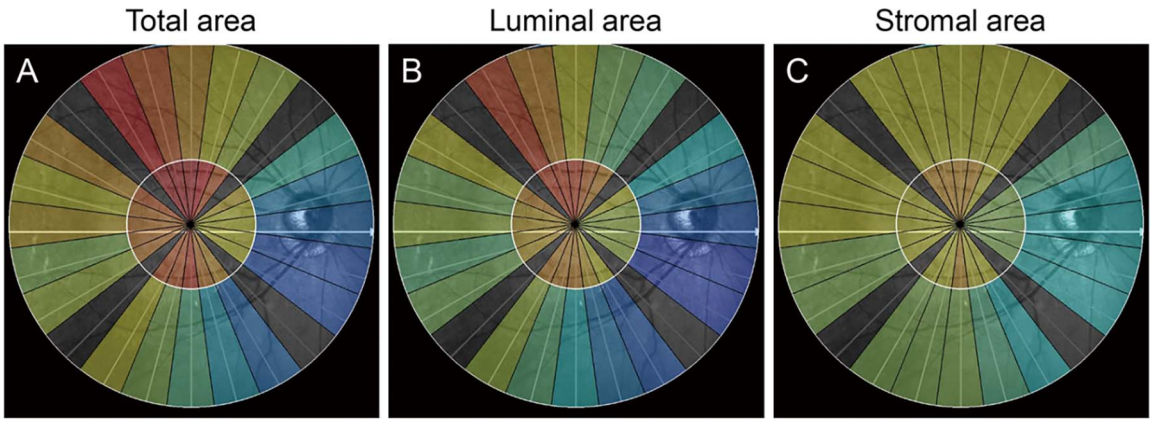

FIGURE 5. Circumferential trend of the total (**A**), luminal (**B**), and stromal (**C**) area in the macular and perimacular zones; *red* represents larger values and *blue* represents smaller values. The total (and luminal) area in the macular area is large and uniform in all four sectors, while that in the perimacular zone is larger in the superior and lateral sectors and smaller in the nasal and inferior sectors (**A**, **B**). Variations of the stromal area are smaller in the macular and perimacular zone than in the total and luminal areas.

the smallest. The nasal sector has the optic nerve, and the choroid becomes thinner toward the optic disc where the choroid disappears.[46,47] Thus, the anatomic factor was thought to be the main cause of this result in the nasal area.

Instead, we compared the choroidal structure of the superior sectors to that of the inferior sectors. As a result, each parameter of the total choroid and luminal and stromal areas was found to be larger in the superior sector than in the inferior sector. This was observed in the macular zone and in the perimacular zone, although the difference was significantly larger in the perimacular zone than in the macular zone. More specifically, the difference of the luminal area was greater than that of the stromal area, which indicated that the larger area of the choroid was mainly due to the larger vascular lumens. The blood in the superior choroid runs to the superior vortex veins, and that in the inferior choroid runs down to the inferior vortex veins. Considering the effect of gravity on the direction of flow, it is possible that the intravascular pressure on the superior choroid is higher than on the inferior choroid. Accordingly, the vascular lumens of the superior choroid are larger or more dilated than in the inferior choroid.

Another possibility is that the differences are innate. Embryologically, the closure of the optic cup ends at the inferior section, which is a common site of a choroidal coloboma.[48] Even though it does not appear as a coloboma, the tissue volume of the choroid in the inferior sector can be smaller than that of the other sectors. Indeed, the stromal area, which is composed of tissue and extracellular matrix, was slightly smaller in the inferior sector than in the superior sector. This embryonic process might play a role in the present findings.

Comparisons to the sectors in the perimacular zone showed significant differences between the superior sector and inferior sector. This difference was not so evident in the macular zone, where the difference of luminal ratio was just 1.16%. If the dilatation of vascular lumen is mainly determined by direction of blood flow, this result is contradictory. Histologically, there is a rich nonvascular smooth muscle cell plexus in the macular choroid.[49,50] This structure may lessen the effect of gravity on circulation of the choroid in the macular area providing sufficient nutritional support to the macula. The retinal thickness is negatively correlated with increasing axial length; however, the foveal retina maintains its thickness irrespective of the axial length.[49] Thus, it is possible that the structure of the fovea, which is the most important area for visual function, is maintained compared to the other area.

The strength of this study is that detailed observations of the choroidal lumen and stroma were made in a wide area of the fundus. This enabled us to analyze the structural characteristics of the choroid in different regions.

Still, this study also had several limitations. First, this study was performed on healthy eyes, and the results cannot be generalized to eyes with diseases. In addition, the distribution of age was not large. Second, to analyze the complex choroidal structure in vivo, we used the binarization technique. This method made it possible to analyze the luminal area and stromal area separately. However, the findings did not provide detailed information especially on the stroma. For example, the luminal area consists of arteries and veins, but this method does not distinguish between them. In addition, it appears that the stroma also contains all the vessel walls, connective tissue, nerves, and inflammatory cells.[39] In the future, more detailed analyses should be carried out for a better understanding of the choroid. Third, there is another limitation of the present method. A closure of binary choroidal circumference lines has been apparently added in some cases. Still, in other instances the dark trace may open up and connect separated vascular lumina. In further cases, the vessel shadow traces create a transection through presumable stromal areas adding a column of pseudo-luminal area. Because of the lack/smaller size of macular epiretinal vessels, these artifacts may affect the macula data less than those from the perimacular regions. The actual bias induced by shadow artifacts toward the luminal component may be small but should be remembered in interpreting the results.

In conclusion, there are significant regional differences in the choroidal structure in normal eyes as seen in the wide-field noninvasive OCT images. The choroid is composed of anastomosing blood vessels so that alterations in the choroidal structure and circulation in a small region can affect the overall

TABLE 5. Coefficient of Variation in Macular Zone and in Perimacular Zone

Coefficient of Variation	Macular Zone	Perimacular Zone	*P* Value
Total area	0.07	0.22	<0.01
Luminal area	0.07	0.12	<0.01
Stromal area	0.08	0.04	<0.01
Luminal ratio	0.01	0.22	<0.01

P values using Mann-Whitney *U* test.

Investigative Ophthalmology & Visual Science

circulation of the choroid. The present method of wide-field OCT will provide important information on the normal conditions and disease-related alterations.

Acknowledgments

The authors thank Duco Hamasaki of Bascom Palmer Eye Institute (University of Miami, FL, USA) for providing critical discussions and suggestions on our study and editing of the final manuscript.

Supported by JSPS KAKENHI Grant 15H04996. The authors alone are responsible for the content and writing of the paper.

Disclosure: **N. Kakiuchi**, None; **H. Terasaki**, None; **S. Sonoda**, None; **H. Shiihara**, None; **T. Yamashita**, None; **M. Tomita**, None; **Y. Shinohara**, None; **T. Sakoguchi**, None; **K. Iwata**, None; **T. Sakamoto**, None

References

1. Castro-Correia J. Understanding the choroid. *Int Ophthalmol*. 1995;19:135–147.
2. Margolis R, Spaide RF. A pilot study of enhanced depth imaging optical coherence tomography of the choroid in normal eyes. *Am J Ophthalmol*. 2009;147:811–815.
3. Yannuzzi LA, Sorenson J, Spaide RF, Lipson B. Idiopathic polypoidal choroidal vasculopathy (IPCV). *Retina*. 2012; 32(suppl 1):1–8.
4. Imamura Y, Fujiwara T, Margolis R, Spaide RF. Enhanced depth imaging optical coherence tomography of the choroid in central serous chorioretinopathy. *Retina*. 2009;29:1469–1473.
5. Kim JH, Kang SW, Kim JR, Kim SJ. Variability of subfoveal choroidal thickness measurements in patients with age-related macular degeneration and central serous chorioretinopathy. *Eye (Lond)*. 2013;27:809–815.
6. Laude A, Cackett PD, Vithana EN, et al. Polypoidal choroidal vasculopathy and neovascular age-related macular degeneration: same or different disease? *Prog Retin Eye Res*. 2010;29: 19–29.
7. Lutty GA, Cao J, McLeod DS. Relationship of polymorphonuclear leukocytes to capillary dropout in the human diabetic choroid. *Am J Pathol*. 1997;151:707–714.
8. Rayess N, Rahimy E, Ying GS, et al. Baseline choroidal thickness as a predictor for response to anti-vascular endothelial growth factor therapy in diabetic macular edema. *Am J Ophthalmol*. 2015;159:85–91.
9. Sonoda S, Sakamoto T, Otsuka H, et al. Responsiveness of eyes with polypoidal choroidal vasculopathy with choroidal hyperpermeability to intravitreal ranibizumab. *BMC Ophthalmol*. 2013;13:43.
10. Sonoda S, Sakamoto T, Yamashita T, et al. Choroidal structure in normal eyes and after photodynamic therapy determined by binarization of optical coherence tomographic images. *Invest Ophthalmol Vis Sci*. 2014;55:3893–3899.
11. Sonoda S, Sakamoto T, Yamashita T, et al. Luminal and stromal areas of choroid determined by binarization method of optical coherence tomographic images. *Am J Ophthalmol*. 2015;159: 1123–1131.
12. Tagawa Y, Namba K, Mizuuchi K, et al. Choroidal thickening prior to anterior recurrence in patients with Vogt-Koyanagi-Harada disease. *Br J Ophthalmol*. 2016;100:473–477.
13. Torres RJ, Luchini A, Both AS, et al. Effect of flaxseed on choroid-sclera complex thickness and on LDL oxidation in the sclera, choroid and retina of diet-induced hypercholesterolaemic rabbits. *Br J Nutr*. 2014;14:112:1438–1446.
14. Nagiel A, Lalane RA, Sadda SR, Schwartz SD. Ultra-widefield fundus imaging: a review of clinical applications and future trends. *Retina*. 2016;36:660–678.
15. Oishi A, Ogino K, Makiyama Y, Nakagawa S, Kurimoto M, Yoshimura N. Wide-field fundus autofluorescence imaging of retinitis pigmentosa. *Ophthalmology*. 2013;120:1827–1834.
16. Hirahara S, Yasukawa T, Kominami A, Nozaki M, Ogura Y. Densitometry of choroidal vessels in eyes with and without central serous chorioretinopathy by wide-field indocyanine green angiography. *Am J Ophthalmol*. 2016;166:103–111.
17. Oishi A, Hidaka J, Yoshimura N. Quantification of the image obtained with a wide-field scanning ophthalmoscope. *Invest Ophthalmol Vis Sci*. 2014;55:2424–2431.
18. Pang CE, Shah VP, Sarraf D, Freund KB. Ultra-widefield imaging with autofluorescence and indocyanine green angiography in central serous chorioretinopathy. *Am J Ophthalmol*. 2014;158:362–371.
19. Lee EK, Lee SY, Yu HG. A clinical grading system based on ultra-wide field retinal imaging for sunset glow fundus in Vogt-Koyanagi-Harada disease. *Graefes Arch Clin Exp Ophthalmol*. 2015;253:359–368.
20. Singh SR, Invernizzi A, Rasheed MA, et al. Wide-field choroidal vascularity in healthy eyes. *Am J Ophthalmol*. 2018;27:193: 100–105.
21. Egawa M, Mitamura Y, Akaiwa K, et al. Changes of choroidal structure after corticosteroid treatment in eyes with Vogt-Koyanagi-Harada disease. *Br J Ophthalmol*. 2016;100:1646–1650.
22. Egawa M, Mitamura Y, Sano H, et al. Changes of choroidal structure after treatment for primary intraocular lymphoma: retrospective, observational case series. *BMC Ophthalmol*. 2015;15:136.
23. Iwata A, Mitamura Y, Niki M, et al. Binarization of enhanced depth imaging optical coherence tomographic images of an eye with Wyburn-Mason syndrome: a case report. *BMC Ophthalmol*. 2015;15:19.
24. Izumi T, Koizumi H, Maruko I, et al. Structural analyses of choroid after half-dose verteporfin photodynamic therapy for central serous chorioretinopathy. *Br J Ophthalmol*. 2017;101: 433–437.
25. Kawano H, Sonoda S, Saito S, Terasaki H, Sakamoto T. Choroidal structure altered by degeneration of retina in eyes with retinitis pigmentosa. *Retina*. 2017;37:2175–2182.
26. Kawano H, Sonoda S, Yamashita T, Maruko I, Iida T, Sakamoto T. Relative changes in luminal and stromal areas of choroid determined by binarization of EDI-OCT images in eyes with Vogt-Koyanagi-Harada disease after treatment. *Graefes Arch Clin Exp Ophthalmol*. 2016;254:421–426.
27. Kinoshita T, Mitamura Y, Mori T, et al. Changes in choroidal structures in eyes with chronic central serous chorioretinopathy after half-dose photodynamic therapy. *PLoS One*. 2016; 11:e0163104.
28. Kinoshita T, Mitamura Y, Shinomiya K, et al. Diurnal variations in luminal and stromal areas of choroid in normal eyes. *Br J Ophthalmol*. 2016;101:360–364.
29. Kinoshita T, Mori J, Okuda N, et al. Effects of exercise on the structure and circulation of choroid in normal eyes. *PLoS One*. 2016;11:e0168336.
30. Nishi T, Ueda T, Mizusawa Y, et al. Choroidal structure in children with anisohypermetropic amblyopia determined by binarization of optical coherence tomographic images. *PLoS One*. 2016;11:e0164672.
31. Sonoda S, Sakamoto T, Kuroiwa N, et al. Structural changes of inner and outer choroid in central serous chorioretinopathy determined by optical coherence tomography. *PLoS One*. 2016;11:e0157190.
32. Branchini LA, Adhi M, Regatieri CV, et al. Analysis of choroidal morphologic features and vasculature in healthy eyes using spectral-domain optical coherence tomography. *Ophthalmology*. 2013;120:1901–1908.

Investigative Ophthalmology & Visual Science

33. Agrawal R, Gupta P, Tan KA, Cheung CM, Wong TY, Cheng CY. Choroidal vascularity index as a measure of vascular status of the choroid: measurements in healthy eyes from a population-based study. *Sci Rep*. 2016;6:21090.
34. Kajić V, Esmaeelpour M, Glittenberg C, et al. Automated three-dimensional choroidal vessel segmentation of 3D 1060 nm OCT retinal data. *Biomed Opt Express*. 2013;4:134–150.
35. Esmaeelpour M, Kajic V, Zabihian B, et al. Choroidal Haller's and Sattler's layer thickness measurement using 3-dimensional 1060-nm optical coherence tomography. *PLoS One*. 2014;9:9:e99690.
36. Bartz-Schmidt KU, Weber J, Heimann K. Validity of two-dimensional data obtained with the Heidelberg Retina Tomograph as verified by direct measurements in normal optic nerve heads. *Ger J Ophthalmol*. 1994;3:400–405.
37. Sonoda S, Sakamoto T, Kakiuchi N, et al. Kago-Eye2 software for semi-automated segmentation of subfoveal choroid of optical coherence tomographic images. *Jpn J Ophthalmol*. 2019;63:82–89.
38. Schneider CA, Rasband WS, Eliceiri KW. NIH image to ImageJ: 25 years of image analysis. *Nat Methods*. 2012;9:671–675.
39. Bron AJ, Tripathi R, Warwick R. The choroid and uveal vessels. In: *Wolff's Anatomy of the Eye and Orbit*. 8th ed. London, UK: Chapman and Hall; 1997:371–410.
40. Hayreh SS. In vivo choroidal circulation and its watershed zones. *Eye (Lond)* 1990;4(pt 2):273–289.
41. Kanda Y. Investigation of the freely available easy-to-use software "EZR" for medical statistics. *Bone Marrow Transplant*. 2013;48:452–458.
42. Ikuno Y, Kawaguchi K, Nouchi T, Yasuno Y. Choroidal thickness in healthy Japanese subjects. *Invest Ophthalmol Vis Sci*. 2010;51:2173–2176.
43. Barteselli G, Chhablani J, El-Emam S, et al. Choroidal volume variations with age, axial length, and sex in healthy subjects: a three-dimensional analysis. *Ophthalmology*. 2012;119:2572–2578.
44. Curcio CA, Sloan KR, Kalina RE, Hendrickson AE. Human photoreceptor topography. *J Comp Neurol*. 1990;22:292:497–523.
45. Jacobson SG, Mcguigan DE III, Sumaroka A, et al. Complexity of the class B phenotype in autosomal dominant retinitis pigmentosa due to rhodopsin mutations. *Invest Ophthalmol Vis Sci*. 2016;57:4847–4858.
46. Kubota T, Jonas JB, Naumann GO. Decreased choroidal thickness in eyes with secondary angle closure glaucoma. An aetiological factor for deep retinal changes in glaucoma? *Br J Ophthalmol*. 1993;77:430–432.
47. Yamashita T, Sakamoto T, Yoshihara N, et al. Correlations between local peripapillary choroidal thickness and axial length, optic disc tilt, and papillo-macular position in young healthy eyes. *PLoS One*. 2017;12:e0186453.
48. Chang L, Blain D, Bertuzzi S, Brooks BP. Uveal coloboma: clinical and basic science update. *Curr Opin Ophthalmol*. 2006;17:447–470.
49. May CA. Non-vascular smooth muscle cells in the human choroid: distribution, development and further characterization. *J Anat*. 2005;207:381–390.
50. Yamashita T, Sakamoto T, Terasaki H, et al. Association of retinal thickness and optic disc-to-fovea angle to axial length of young healthy eyes. *Clin Ophthalmol*. 2015;9:2235–2241.

Investigative Ophthalmology & Visual Science